PERGAMON

International Journal of Heat and Mass Transfer 43 (2000) 1767–1776

International Journal of HEAT and MASS TRANSFER

www.elsevier.com/locate/ijhmt

Solution of the inverse radiation problem using a conjugate gradient method

H.M. Park*, T.Y. Yoon

Department of Chemical Engineering, Sogang University, Seoul, South Korea

Received 1 February 1999; received in revised form 3 August 1999

Abstract

An inverse radiation analysis is presented for estimating radiative parameters from the temperature measurement in three-dimensional participating media, where radiation and conduction occur simultaneously. The S_N method is employed to solve the radiative transfer equation. The inverse radiation problem is solved through the minimization of a performance function, which is expressed by the sum of square residuals between calculated and observed temperature, utilizing the conjugate gradient method. The present technique is robust and yields accurate estimation of radiative parameters even with noisy measurement of temperature. © 2000 Elsevier Science Ltd. All rights reserved.

1. Introduction

One of the most important mechanisms of heat transfer in high temperature equipments is radiation. Since the radiation effects the temperature field, the actual mode of heat transfer in most cases is combined radiation and conduction or convection. In the present investigation, we consider heat transfer by combined conduction with radiation through participating media capable of absorbing, emitting and scattering thermal radiation. In this case, the energy conservation equation provides the local temperature which determines the blackbody intensity in the radiative transfer equation. On the other hand, the divergence of the radiative flux that is present as a source term in the energy conservation equation is obtained only after solving the radiative transfer equation. Thus, the problems are always implicit in temperature, and therefore, require iterative procedure which makes the modeling of these processes challenging. Another difficulty encountered in the modeling of these processes is the estimation of radiative properties of the medium. Although several reliable numerical methods are available for the solution of the radiative transfer equation, accurate prediction of the radiation field is not possible without employing accurate values of these radiative parameters. Inverse radiation analysis is concerned with the determination of the radiative properties from various types of measurements [1–3]. In the present work, we develop a method of solving three-dimensional inverse radiation problems which allows one to estimate the radiative parameters from the measurement of temperature. On the one hand, the strong coupling of the radiation and the temperature fields makes the analysis complicated, but on the other hand it allows the estimation of radiative parameters from the relatively easier measurement of temperature. The radiative transfer equation is solved by using the S_N method with $N = 4$ in the present investigation.

* Corresponding author. Tel.: +82-2705-8482.

0017-9310/00/$ - see front matter
PII: S0017-9310(99)00255-0

Nomenclature

a_i	linear anisotropic coefficient (Eq. (8))
$\boldsymbol{d}$	conjugate direction vector
D	width of the system (m)
G	incident radiation
H	height of the system (m)
I	radiation intensity
I_b	blackbody intensity
J	performance function (Eq. (15))
k	thermal conductivity (W/m K)
MO	number of measurement points
$\hat{\boldsymbol{n}}$	unit inward normal vector
$\boldsymbol{P}$	parameter vector (κ, σ)
$\boldsymbol{q}_r$	radiative heat flux
$\hat{\boldsymbol{s}}$	unit vector into a given direction
T	temperature field
$T^\dagger$	observed temperature field
W_m	angular quadrature weight associated with the mth direction

Greek symbols

ϵ	emissivity
η_m	direction cosine
κ	absorption coefficient
μ_m	direction cosine
ξ_m	direction cosine
ρ	optimal step length in the conjugate gradient method
σ	scattering coefficient
σ_b	Stefan–Boltzmann constant, $\sigma_b = 5.670 \times 10^{-8}$ W/m^2 K^4
σ_e	error adjusting parameter (Eq. (30))
$\Phi_{m'm}$	scattering phase function
ψ	parameter defined by Eq. (24)
ω	random number
Ω	solid angle

2. The system and governing equations

The system under consideration is depicted in Fig. 1(a), which is a rectangular enclosure containing participating media with opaque and diffusively reflecting boundaries. Heat transfer in this system is contributed by conduction as well as radiation with absorption, scattering and emission. The steady temperature field in this enclosure is governed by the following equation.

$$k\nabla^2 T - \nabla \cdot \boldsymbol{q}_r = 0 \tag{1}$$

where k (=44 W/m K) is the thermal conductivity, T is the temperature and $\boldsymbol{q}_r$ is the radiative heat flux. The boundary conditions for Eq. (1) are given as:

$$x = 0, \quad T = 900$$

$$x = D, \quad T = 900$$

$$y = 0, \quad T = 900$$

$$y = L, \quad T = 900$$

$$z = 0, \quad T = 1200$$

$$z = H, \quad T = 400 \tag{2}$$

where D = 2 m, L = 2 m, and H = 4 m. The divergence of radiative heat flux $\nabla \cdot \boldsymbol{q}_r$ in Eq. (1) is determined by the following equation.

$$\nabla \cdot \boldsymbol{q}_r = 4\pi\kappa\left(I_b - \frac{G}{4\pi}\right) \tag{3}$$

where κ is the absorption coefficient, I_b is the Planck function (blackbody intensity) and G is the incident radiation, which are given by the following equations.

$$G \equiv \int_{4\pi} I(\boldsymbol{r}, \hat{\boldsymbol{s}})\, \mathrm{d}\Omega \tag{4a}$$

$$I_b = \frac{\sigma_b}{\pi} T^4 \tag{4b}$$

Here, σ_b is the Stefan–Boltzmann constant, and $I(\boldsymbol{r}, \hat{\boldsymbol{s}})$ is the radiation intensity which is governed by the following radiative transfer equation for participating media with absorption, emission and scattering:

$$\nabla \cdot (\hat{\boldsymbol{s}} I) + (\kappa + \sigma) I = \kappa I_b + \frac{\sigma}{4\pi} \int_{4\pi} I(\boldsymbol{r}, \hat{\boldsymbol{s}}') \Phi(\hat{\boldsymbol{s}} \cdot \hat{\boldsymbol{s}}')\, \mathrm{d}\Omega \tag{5}$$

where Φ is the scattering phase function, $\hat{\boldsymbol{s}}$ is a unit vector in the direction of the radiation, Ω is the solid angle and σ is the scattering coefficient. The relevant boundary conditions for Eq. (5) at the boundary walls are as follows:

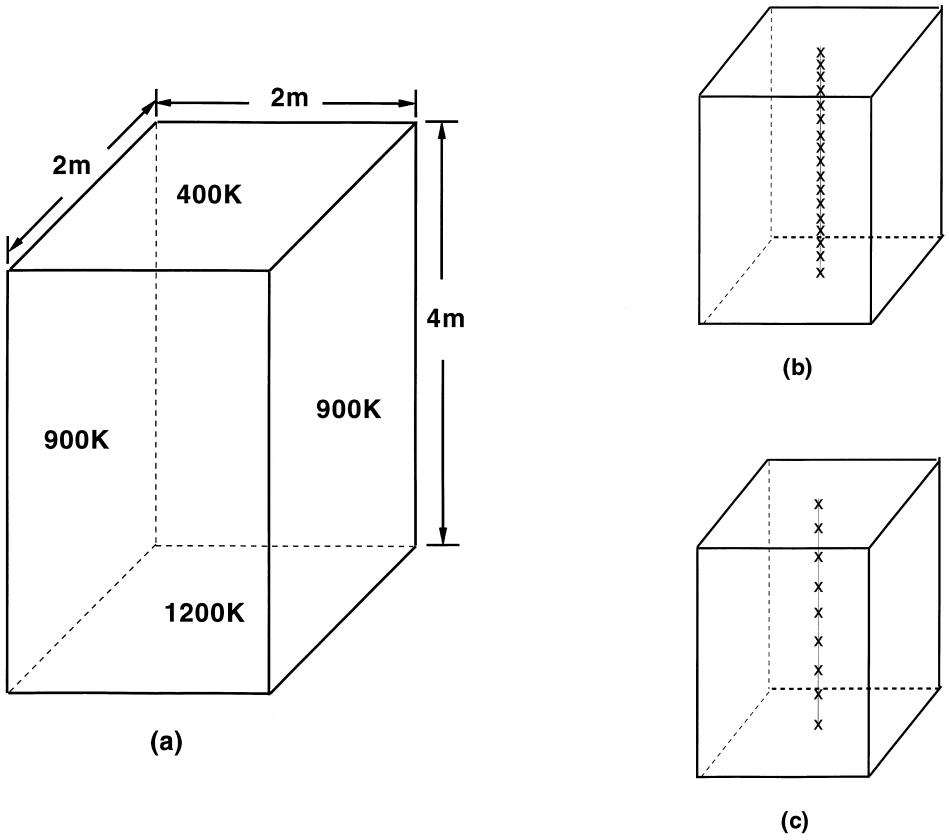

Fig. 1. (a) The system; (b) the location of 17 measurement points; and (c) the location of nine measurement points.

$$I(\boldsymbol{r}_w,\hat{\boldsymbol{s}}) = \epsilon(\boldsymbol{r}_w)I_b(\boldsymbol{r}_w) + \frac{1-\epsilon(\boldsymbol{r}_w)}{\pi}\int_{\hat{\boldsymbol{n}}\cdot\hat{\boldsymbol{s}}'<0} I(\boldsymbol{r}_w,\hat{\boldsymbol{s}}')|\hat{\boldsymbol{n}}\cdot\hat{\boldsymbol{s}}'|\,d\Omega' \quad (\hat{\boldsymbol{n}}\cdot\hat{\boldsymbol{s}}>0) \tag{6}$$

where $\hat{\boldsymbol{n}}$ is the inward normal vector, $\hat{\boldsymbol{s}}'$ is the unit vector in the incoming beam direction and $\epsilon(\boldsymbol{r}_w)$ is the wall emissivity.

When the S_N method with $N=4$ (S_4 method) is applied to Eq. (5), it is discretized as follows [4]:

$$\mu_m\frac{\partial I^m}{\partial x} + \xi_m\frac{\partial I^m}{\partial y} + \eta_m\frac{\partial I^m}{\partial z} = -(\kappa+\sigma)I^m + \kappa I_b + \frac{\sigma}{4\pi}\sum_{m'=1}^{Nm'} W_{m'}\Phi_{m'm}I^{m'} \tag{7}$$

where I_m ($\equiv I(x, y, z; \mu_m, \xi_m, \eta_m)$) is the total radiation intensity at the position (x, y, z) in the discrete direction given by the direction cosine (μ_m, ξ_m, η_m), $W_{m'}$ is the angular quadrature weight associated with the m'th direction, and $\Phi_{m'm}$ is the discretized phase function for scattering between m' and m discrete directions. In the present investigation linear anisotropic scattering is assumed

$$\Phi_{m'm} = 1.0 + a_1(\mu_m\mu_{m'} + \xi_m\xi_{m'} + \eta_m\eta_{m'}) \tag{8}$$

The value a_1 is the asymmetric factor that lies between $-1 \le a_1 \le 1$, where the values -1, 0 and 1 denote backward, isotropic and forward scattering, respectively. The boundary conditions given by Eq. (6), representing the diffusively emitting and reflecting walls, are discretized by means of the S_4 method as follows:

$$x=0,\quad I^m = \epsilon I_b + \frac{1-\epsilon}{\pi}\sum_{\mu_{m'}<0} W_{m'}|\mu_{m'}|I^{m'} \quad (\mu_m>0) \tag{9}$$

$$x=D,\quad I^m = \epsilon I_b + \frac{1-\epsilon}{\pi}\sum_{\mu_{m'}>0} W_{m'}|\mu_{m'}|I^{m'} \quad (\mu_m<0) \tag{10}$$

$$y=0,\quad I^m=\epsilon I_b+\frac{1-\epsilon}{\pi}\sum_{\xi_{m'}<0}W_{m'}|\xi_{m'}|I^{m'} \qquad (\xi_m>0) \tag{11}$$

$$y=L,\quad I^m=\epsilon I_b+\frac{1-\epsilon}{\pi}\sum_{\xi_{m'}>0}W_{m'}|\xi_{m'}|I^{m'} \qquad (\xi_m<0) \tag{12}$$

$$z=0,\quad I^m=\epsilon I_b+\frac{1-\epsilon}{\pi}\sum_{\eta_{m'}<0}W_{m'}|\eta_{m'}|I^{m'} \qquad (\eta_m>0) \tag{13}$$

$$z=H,\quad I^m=\epsilon I_b+\frac{1-\epsilon}{\pi}\sum_{\eta_{m'}>0}W_{m'}|\eta_{m'}|I^{m'} \qquad (\eta_m<0) \tag{14}$$

Here, I^m is the intensity of radiation leaving the wall, ϵ is the surface emissivity and I_b is the total blackbody radiation intensity at the temperature of the wall. Eqs. (1) and (5) are coupled through the terms $\nabla\cdot\boldsymbol{q}_r$ and I_b, and must be solved iteratively to yield the radiation and the temperature fields. The computational procedure is as follows:

1. Assume the temperature field.
2. Calculate I_b using the given temperature field.
3. Solve the radiative transfer Eq. (5) to obtain the radiation intensity I.
4. The divergence of the radiative heat flux is determined by Eq. (3).
5. Solve Eq. (1) to obtain the temperature field.
6. If the radiation and the temperature fields are not converged, go to the Step 2.

3. The inverse radiation problem

The temperature field inside the domain, which can be easily measured at various locations, is influenced by the radiation field through the term $\nabla\cdot\boldsymbol{q}_r$ (cf. Eqs. (1), (3), (4a) and (4b)). Conversely, the radiation intensity is affected by the temperature field through I_b (cf. Eq. (5)) and by the radiative parameters such as absorption coefficient, scattering coefficient and the linear anisotropic coefficient. Therefore, the radiative parameters can be estimated by using the measured values of the temperature field at certain locations. The performance function for the identification of the radiative parameters is expressed by the sum of square residuals between the calculated and the observed temperature as follows:

$$J=\frac{1}{2}\sum_{m=1}^{MO}\Big[T(x_m,y_m,z_m;\boldsymbol{P})-T^{\dagger}(x_m,y_m,z_m)\Big]^2 \tag{15}$$

where $T(x_m, y_m, z_m; \boldsymbol{P})$ is the calculated temperature at the location (x_m, y_m, z_m) with the radiative parameters $\boldsymbol{P}=(\kappa,\sigma)^{\mathrm{T}}$, $T^{\dagger}(x_m, y_m, z_m)$ is the observed temperature at the same location, and MO is the total number of measurement points. The problem of inverse radiation now becomes the minimization of the performance function, Eq. (15), over the parameter vector $\boldsymbol{P}$. The minimization procedure is performed using a conjugate gradient method suggested by Fletcher and Reeves [5]. The variation of the performance function with respect to the parameter vector $\boldsymbol{P}$ is determined by the following gradient vector.

$$\left(\frac{\partial J}{\partial \boldsymbol{P}}\right)^{\mathrm{T}}=\left(\frac{\partial J}{\partial P_1},\frac{\partial J}{\partial P_2},\ldots,\frac{\partial J}{\partial P_N}\right) \tag{16}$$

where

$$\frac{\partial J}{\partial \boldsymbol{P}}=\sum_{m=1}^{MO}\Big[T(x_m,y_m,z_m;\boldsymbol{P})-T^{\dagger}(x_m,y_m,z_m)\Big]\frac{\partial T(x_m,y_m,z_m;\boldsymbol{P})}{\partial \boldsymbol{P}} \tag{17}$$

and N is the number of radiative parameters to be estimated. The governing equations for the sensitivity functions $[\partial T/\partial \boldsymbol{P}]^{\mathrm{T}}=(\partial T/\partial P_1,\ \partial T/\partial P_2,\ldots,\partial T/\partial P_N)$, which represent the variation of the temperature field with respect to the vector $\boldsymbol{P}$, are obtained by partially differentiating Eqs. (1) and (7) with respect to the parameter vector. Differentiating Eq. (1) with respect to $\boldsymbol{P}$, we find

$$k\nabla^2\left(\frac{\partial T}{\partial \boldsymbol{P}}\right)-\frac{\partial}{\partial \boldsymbol{P}}(\nabla\cdot\boldsymbol{q}_r)=0 \tag{18}$$

with the following condition at all boundaries

$$\frac{\partial T}{\partial \boldsymbol{P}}=0 \tag{19}$$

For the determination of the second term in Eq. (18), we need the governing equation for $(\partial I^m/\partial \boldsymbol{P})$.

$$\mu_m\frac{\partial}{\partial x}\left(\frac{\partial I^m}{\partial \boldsymbol{P}}\right)+\xi_m\frac{\partial}{\partial y}\left(\frac{\partial I^m}{\partial \boldsymbol{P}}\right)+\eta_m\frac{\partial}{\partial z}\left(\frac{\partial I^m}{\partial \boldsymbol{P}}\right)=-\left(\frac{\partial}{\partial \boldsymbol{P}}(\kappa+\sigma)\right)I^m-(\kappa+\sigma)\left(\frac{\partial I^m}{\partial \boldsymbol{P}}\right)$$

$$+\left(\frac{\partial}{\partial \boldsymbol{P}}\kappa\right)I_{\mathrm{b}}+\kappa\frac{\partial I_{\mathrm{b}}}{\partial \boldsymbol{P}}+\frac{1}{4\pi}\left(\frac{\partial \sigma}{\partial \boldsymbol{P}}\right)\sum_{m'=1}^{Nm'}W'_{m}\Phi_{m'm}I^{m'}$$

$$+\frac{\sigma}{4\pi}\sum_{m'=1}^{Nm'}W'_{m}\Phi_{m'm}\left(\frac{\partial I^{m'}}{\partial \boldsymbol{P}}\right) \tag{20}$$

The relevant boundary conditions for Eq. (20) are also obtained by partially differentiating Eqs. (9)–(14) with respect to $\boldsymbol{P}$. For example,

$x=0$,

$$\frac{\partial I^{m}}{\partial \boldsymbol{P}}=\epsilon\left(\frac{\partial I_{\mathrm{b}}}{\partial \boldsymbol{P}}\right)+\frac{1-\epsilon}{\pi}\sum_{\mu_{m'}<0}W_{m'}|\mu_{m'}|\left(\frac{\partial I^{m'}}{\partial \boldsymbol{P}}\right) \tag{21}$$

$$\left(\mu_{m}>0\right)$$

Boundary conditions at other walls can be obtained in a similar way. Since $I_{\mathrm{b}}=\sigma_{\mathrm{b}}T^{4}/\pi$, we find

$$\frac{\partial I_{\mathrm{b}}}{\partial \boldsymbol{P}}=\frac{4\sigma_{\mathrm{b}}T^{3}}{\pi}\left(\frac{\partial T}{\partial \boldsymbol{P}}\right) \tag{22a}$$

The second term in Eq. (18) is evaluated as:

$$\frac{\partial}{\partial \boldsymbol{P}}(\nabla\cdot\boldsymbol{q}_{\mathrm{r}})=4\pi\left(\frac{\partial \kappa}{\partial \boldsymbol{P}}\right)\left(I_{\mathrm{b}}-\frac{G}{4\pi}\right)+4\pi\kappa\left(\frac{\partial I_{\mathrm{b}}}{\partial \boldsymbol{P}}-\frac{1}{4\pi}\int_{\Omega}\frac{\partial I}{\partial \boldsymbol{P}}\,\mathrm{d}\Omega\right) \tag{22b}$$

Therefore, Eqs. (18) and (20) are coupled and must be solved iteratively in a similar manner to the case of Eqs. (1) and (5) as explained in Section 2. The set of equations in Eq. (20) is solved by using the S_4 method.

The conjugate direction or the search direction $\boldsymbol{d}$ is calculated and renewed by the Fletcher–Reeves method:

$$\boldsymbol{d}^{(i+1)}=-\left[\frac{\partial J}{\partial \boldsymbol{P}}\right]^{(i+1)}+\psi\boldsymbol{d}^{(i)}\quad(i\geq 0) \tag{23}$$

where

$$\psi=\frac{\sum_{n=1}^{N}\left[\left(\frac{\partial J}{\partial P_{n}}\right)^{(i+1)}\right]^{2}}{\sum_{n=1}^{N}\left[\left(\frac{\partial J}{\partial P_{n}}\right)^{(i)}\right]^{2}} \tag{24}$$

On the other hand, the search direction at the first step is computed by:

$$\boldsymbol{d}^{(0)}=-\frac{\partial J}{\partial \boldsymbol{P}} \tag{25}$$

This renewed $\boldsymbol{d}^{(i+1)}$ is used for the search direction at the next iteration state. The parameter vector $\boldsymbol{P}^{(i+1)}$ at the $(i+1)$th iterative state is obtained from $\boldsymbol{P}^{(i)}$ by moving in the conjugate direction $\boldsymbol{d}^{(i)}$.

$$\boldsymbol{P}^{(i+1)}=\boldsymbol{P}^{(i)}+\rho\boldsymbol{d}^{(i)} \tag{26}$$

The optimal step length ρ is determined by minimizing $J(\boldsymbol{P}+\rho\boldsymbol{d})$ with respect to ρ. Exploiting the following formula

$$T(\boldsymbol{P}+\rho\boldsymbol{d})=T(\boldsymbol{P})+\left(\frac{\partial T}{\partial \boldsymbol{P}}\right)^{T}\cdot\rho\boldsymbol{d} \tag{27}$$

we find, after some algebraic manipulation, the expression for the optimal step length.

$$\rho=-\frac{\sum_{m=1}^{MO}\left[\left(T(x_{m},y_{m},z_{m})-T^{\dagger}(x_{m},y_{m},z_{m})\right)\sum_{n=1}^{N}\left(\frac{\partial T(x_{m},y_{m},z_{m})}{\partial P_{n}}d_{n}\right)\right]}{\sum_{m=1}^{MO}\left(\sum_{n=1}^{N}\frac{\partial T(x_{m},y_{m},z_{m})}{\partial P_{n}}d_{n}\right)^{2}} \tag{28}$$

where d_n is the nth component of the conjugate direction vector $\boldsymbol{d}$, i.e.,

$$\boldsymbol{d}^{\mathrm{T}}=(d_{1},d_{2},\ldots,d_{N}) \tag{29}$$

The procedure for the conjugate gradient method is summarized as follows:

1. Assume the parameter vector $\boldsymbol{P}=(P_1, P_2,\ldots, P_N)^{\mathrm{T}}$. Solve Eqs. (1) and (5) iteratively to obtain T and I. Similarly, solve Eqs. (18) and (20) iteratively to obtain $\partial T/\partial \boldsymbol{P}$ and $\partial I/\partial \boldsymbol{P}$.
2. Calculate $\boldsymbol{d}^{(0)}=-(\partial J/\partial \boldsymbol{P})$ by using Eq. (17).
3. Determine the optimal step length by using Eq. (28).
4. Calculate $\boldsymbol{P}^{(i+1)}$ by using Eq. (26).
5. Obtain T and I by solving Eqs. (1) and (5) iteratively. Similarly solve Eqs. (18) and (20) iteratively to obtain $\partial T/\partial \boldsymbol{P}$ and $\partial I/\partial \boldsymbol{P}$.
6. Calculate ψ by using Eq. (24).
7. Calculate $\boldsymbol{d}^{(i+1)}$ by using Eq. (23). If $|\boldsymbol{d}^{(i+1)}|$ is less than a prescribed small number, stop the procedure.
8. Set $i=i+1$ and go to the Step 3.

4. Results

Before estimating parameters of a system, we need experimental measurements from the system. We solved the governing equation of the system with ($11\times 11\times 17$) grid numbers to obtain numerical solutions.

We then use these numerical solutions as experimental measurements after adding small random noise. It is expected that the accuracy of the estimation of parameters improves as the number of measurement points increases, but we have to be satisfied with a finite number of measurement points in a typical experiment. As the default measurement points, we select 17 points which are distributed axially as shown in Fig. 1(b). All results presented in this section are obtained by using these default measurement points, if not specified otherwise.

When experimental measurements are obtained, they are subject to measurement errors due to inaccuracy of the instruments and to external random disturbances. If the numerical solution of the governing equation is adopted as experimental measurements, the effect of noise is taken into account artificially as in the following equation.

$$T_{\text{measured}}\left(=T^{\dagger}\right)=T_{\text{exact}}+\omega\sigma_{\text{e}} \tag{30}$$

where σ_{e} determines the noise level, which takes values of 0.0, 3.0, 4.0, 5.0 and ω is a random number between $-2.576\leq\omega\leq2.576$. In fact, σ_{e} is the standard deviation of measurement errors which is assumed to be the same for all measurements, and ω is the Gaussian distributed random error. The above range of ω value corresponds to 99% confidence bound for the temperature measurement.

As a first demonstration of the present technique of parameter estimation, the absorption coefficient κ and the scattering coefficient σ are estimated, respectively, using the simulated experimental data. The exact value of κ is 0.5 and that of σ is also 0.5, if not specified otherwise. Fig. 2(a) shows the convergence of the iteration procedure of conjugate gradient method when κ is estimated with a known value of σ ($=0.5$), assuming that there is no measurement error. For various initial approximations of κ, accurate predictions of κ are obtained after five iterations. Similarly, Fig. 2(b) plots the convergence rate of the estimation of σ when a known value of κ ($=0.5$) is employed. The scattering coefficient σ is also predicted accurately after five iterations for various initial approximations of σ.

As explained in the previous section, one of the most important ingredients of the conjugate gradient method

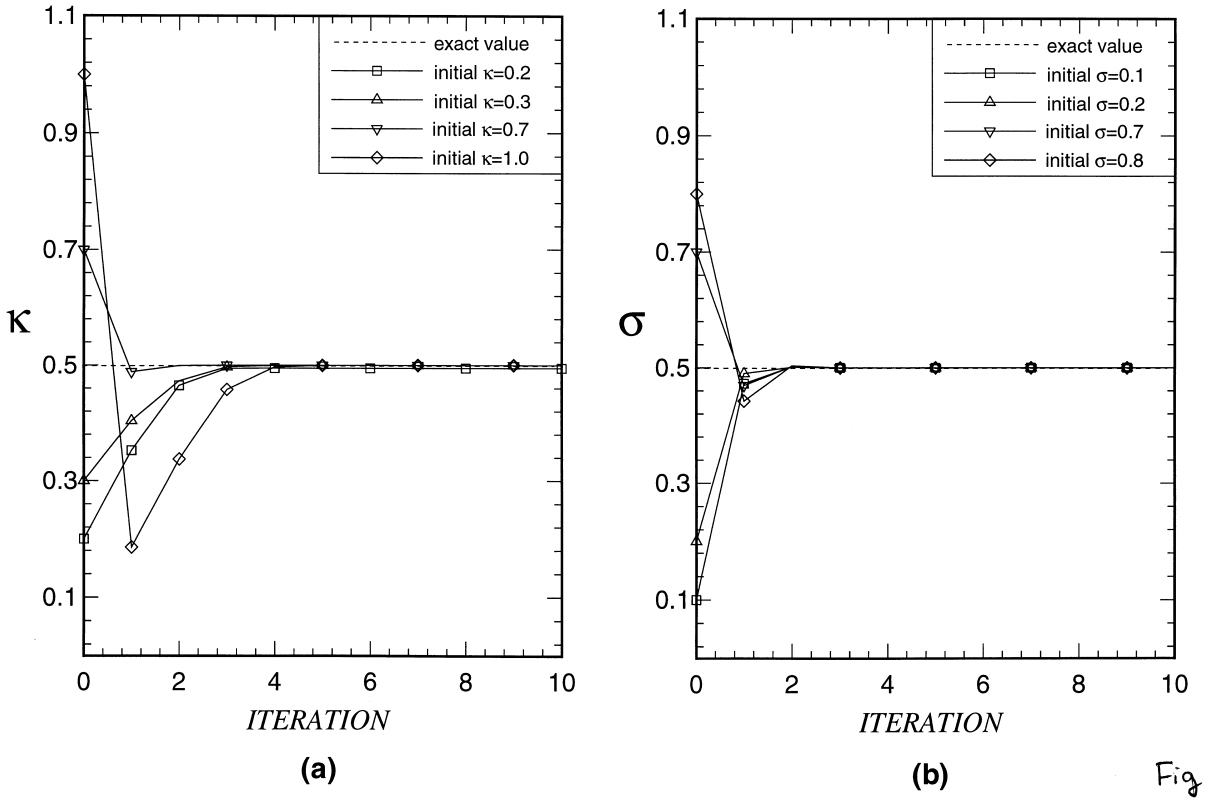

Fig. 2. Convergence of the iteration procedure of the conjugate gradient method. (a) Absorption coefficient and (b) scattering coefficient.

is the evaluation of $\partial J/\partial \boldsymbol{P}$, which indicates the variation of the performance index J with respect to the parameter $\boldsymbol{P}$. This gradient vector is determined by the sensitivity functions ($\partial T/\partial \boldsymbol{P}$), which represent the variation of the temperature field with respect to the parameter vector $\boldsymbol{P}$ (cf. Eq. (17)). Fig. 3(a)–(d) show the field $\partial T/\partial \kappa$ at $y =$ 1 m at various iteration numbers when the initial approximation of $\kappa = 0.2$. As the iteration progresses, the estimated value of the parameter κ approaches the exact one and the magnitude of $\partial T/\partial \kappa$ decreases. Similar figures for the field $\partial T/\partial \sigma$ are displayed in Fig. 3(e)–(h) when the initial approximation of $\sigma = 0.2$. The variation of the magnitude of $\partial T/\partial \sigma$ with respect to the iteration number shows the same tendency. Fig. 3(a)–(h) reveal that the magnitude of $\partial T/\partial \kappa$ is much larger than that of $\partial T/\partial \sigma$ at the same deviation of the estimated parameter values from the exact ones. Because the sensitivity of the temperature field to κ is much larger than that to σ, the simultaneous estimation of κ and σ does not work unless the initial approximation of these parameters are near the exact values. To overcome this difficulty, we employ the following two-stage estimation. At the first stage, we assume the value of the lesser sensitive parameter, σ, and perform the estimation procedure to obtain the converged value of the more sensitive parameter κ. Since the temperature field is not very sensitive to the scattering coefficient σ, we can still obtain converged estimation of κ which is not far from the exact value. Comparing Fig. 3(c), (d) and (e)–(h), we find that the magnitude of $\partial T/\partial \kappa$ field decreases approximately to that of $\partial T/\partial \sigma$ when the estimated value of κ is near the exact one. Next, using the assumed value of σ and the converged estimation of κ from the first stage, we perform the simultaneous estimation of κ and σ, which constitutes the second stage of the procedure. Fig. 4(a)–(d) show the results based on this two stage procedure when

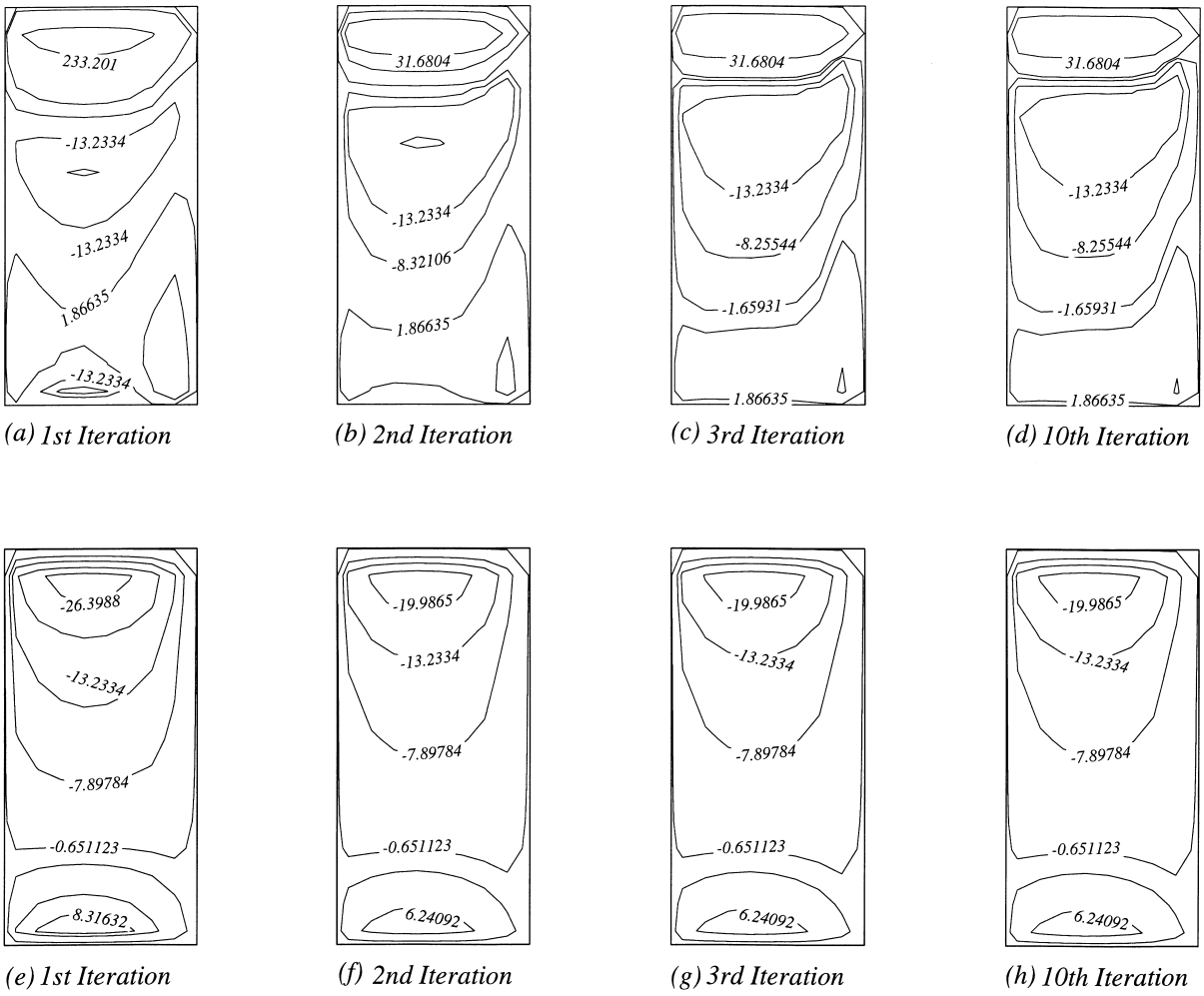

Fig. 3. Sensitivity fields at $y = 1.0$ m at various iteration numbers. (a)–(d) $\partial T/\partial \kappa$ and (e)–(h) $\partial T/\partial \sigma$.

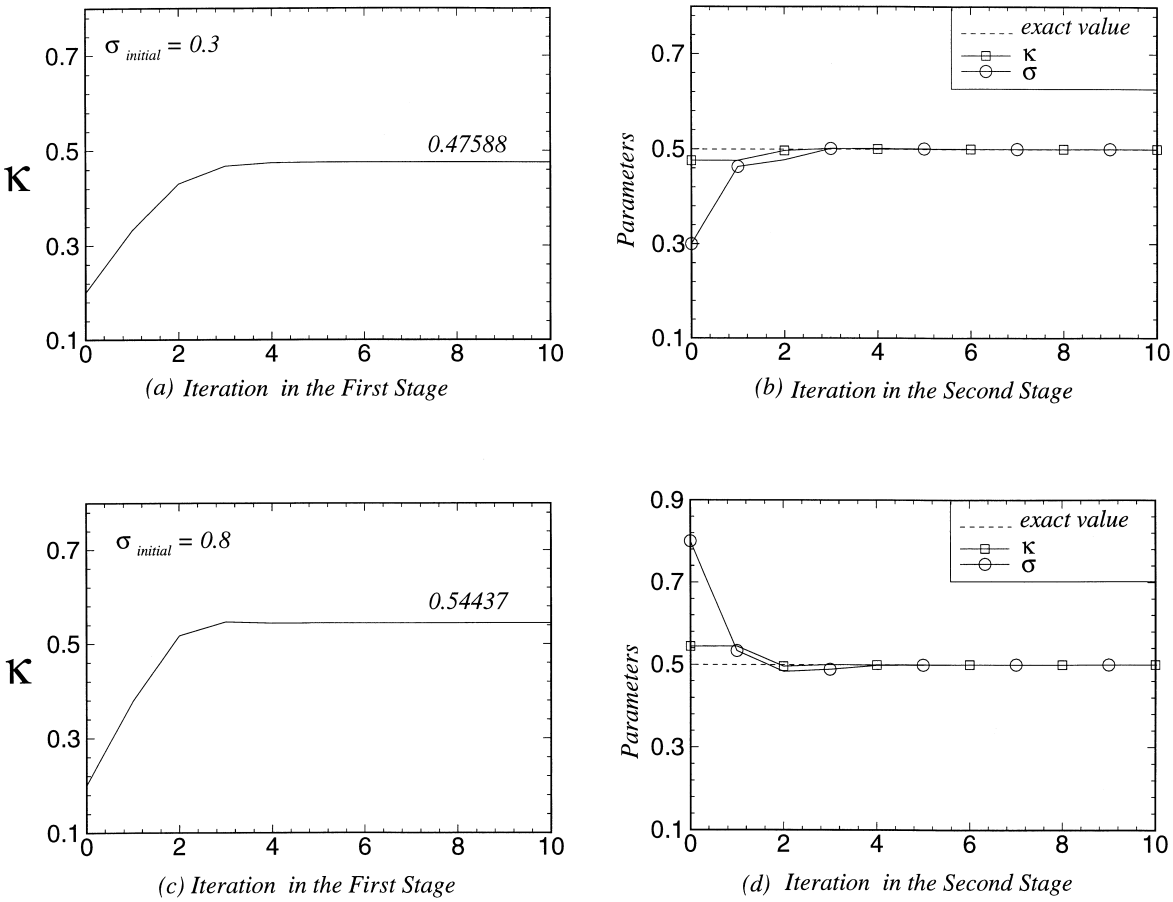

Fig. 4. Two-stage procedure : (a) the first stage when $\sigma_{\text{initial}} = 0.3$; (b) the second stage when $\sigma_{\text{initial}} = 0.3$; (c) the first stage when $\sigma_{\text{initial}} = 0.8$; and (d) the second stage when $\sigma_{\text{initial}} = 0.8$.

there is no measurement error. Fig. 4(a) shows the result of the first stage when the initial approximation of σ is 0.3. The first stage yields $\kappa = 0.47588$ as the converged estimated value. When the second stage iteration is performed using $\sigma = 0.3$ and $\kappa = 0.47588$ as initial approximations, it yields almost exact estimation for these parameters as shown in Fig. 4(b). Fig. 4(c) and (d) are similar results when the initial assumption of σ is 0.8. It is shown that this two-stage procedure yields very accurate results regardless of the initial approximation of the lesser sensitive parameter, σ.

Fig. 5(a) and (b) show the effect of noise level σ_e on the accuracy of the estimation. These figures show that the accuracy of the estimation deteriorates as the noise level σ_e increases. Finally, the effect of number of measurement points on the accuracy of the estimation is investigated. Fig. 6(a) and (b) show the estimated values of κ and σ, respectively, for various noise level σ_e when the number of measurement points is reduced to 9, as depicted in Fig. 1(c), instead of the default value of 17. Comparing Figs. 5 and 6, it is found that the reduction of number of measurement points does not affect the accuracy of the estimation when the noise level σ_e is low. For larger value of the noise level ($\sigma_e > 4$), the estimation is still reasonable when the number of measurement points is 17 (Fig. 5) but the estimation becomes worse rapidly with the employment of nine measurement points (Fig. 6).

5. Conclusion

The inverse radiation problem of estimating radiative parameters from the temperature measurement within the participating media is investigated by employing the conjugate gradient method. The strong coupling of the radiation and the temperature fields allows the estimation of radiative parameters from the relatively

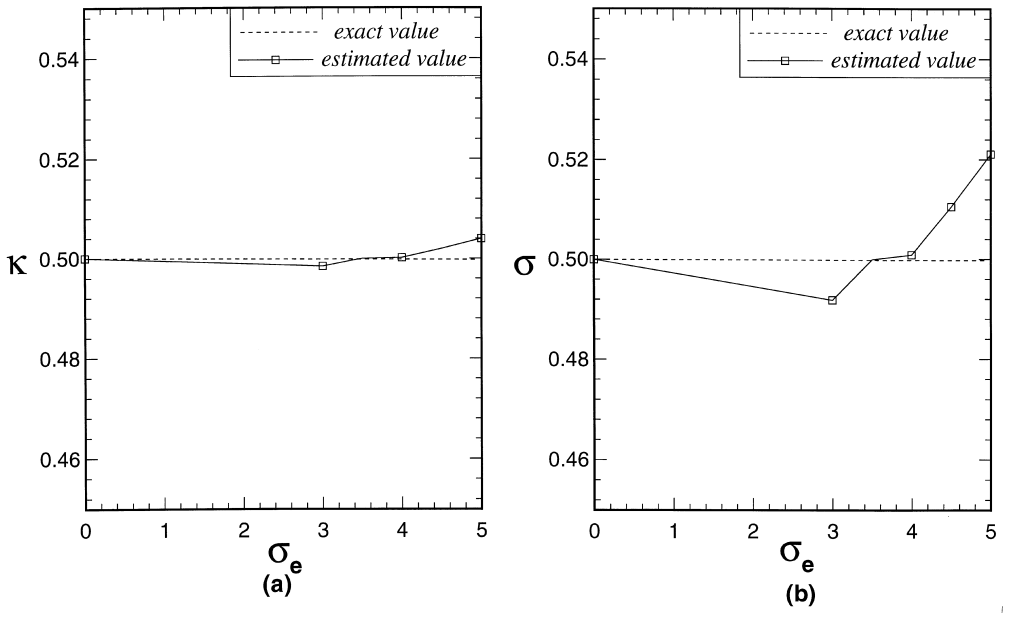

Fig. 5. Effect of noise level σ_e on the accuracy of the estimation. (a) Absorption coefficient and (b) scattering coefficient.

easier measurement of temperature. The S_4 method is used to solve the radiative transfer equation and the corresponding sensitivity equation. The present technique is robust and yields accurate estimation of radiative parameters even with noisy measurement of temperature.

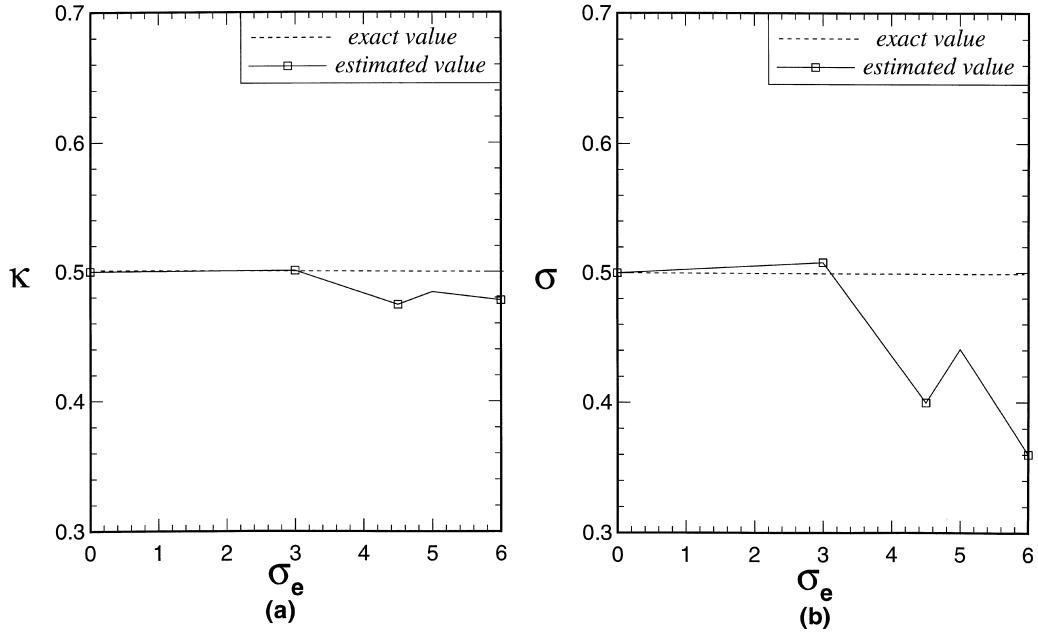

Fig. 6. Accuracy of the estimation when using nine measurement points (cf. Fig. 1(c)). (a) Absorption coefficient and (b) scattering coefficient.

Acknowledgements

We acknowledge the financial support of R&D Management Center for Energy and Resources (R.A.C.E.R).

References

[1] C.H. Ho, M.N. Özisik, An inverse radiation problem, International Journal of Heat and Mass Transfer 32 (1989) 335–341.

[2] K. Kamiuto, An iterative method for inverse scattering problems, Journal of Quantitative Spectroscopy and Radiative Transfer 49 (1993) 1–13.

[3] N.J. McCormick, Inverse radiative transfer problems: a review, Nuclear Science and Engineering 112 (1992) 185–198.

[4] W.A. Fiveland, Three-dimensional radiative heat-transfer solutions by discrete-ordinates method, Journal of Thermophysics and Heat-Transfer 2 (4) (1988) 309–316.

[5] R. Fletcher, R.M. Reeves, Function minimization by conjugate gradients, The Computer Journal 7 (1964) 149–154.